

Energy dissipation in sheared wet granular assemblies

S. Karmakar,¹ M. Schaber,¹ A.-L. Schuhmacher,¹ M. Scheel,^{2,3} M. DiMichiel,² M. Brinkmann,¹ R. Seemann,¹ L. Kovalcinova,⁴ and L. Kondic⁴

¹*Experimental Physics, Saarland University, Saarbrücken, D-66123, Germany*

²*European Synchrotron Radiation Facility, Grenoble, F-38043, France*

³*Synchrotron Soleil, 91192 Gif-sur-Yvette, France*

⁴*Department of Mathematical Sciences, New Jersey Institute of Technology, New Jersey, USA*

(Dated: March 27, 2017)

Energy dissipation in sheared dry and wet granulates is explored experimentally and computationally as a function of confining pressure P_{cf} . For vanishing confining pressure, $P_{cf} \rightarrow 0$, the energy dissipation fades in the case of dry granulates. In the case of wet granulates, a finite energy dissipation for $P_{cf} \rightarrow 0$ is observed and explained quantitatively by a combination of two effects related to capillary forces: frictional resistance of the granulate in presence of an internal cohesion by virtue of attractive capillary forces and energy dissipation due to the rupture and reformation of liquid bridges. With increasing P_{cf} the energy dissipation for both dry and wet granulates grows in a linear fashion due to particle–particle friction. Because of a lower Coulomb friction coefficient in the case of a wet granulate, a cross-over is observed for sufficiently large P_{cf} where more energy is dissipated in a dry granulate.

The mechanics of wet granulates play a prominent role in various fields of process engineering, including the production of pharmaceuticals [6–8], wet granulation of powders [6–8], sintering [9] and food production [10]. Owing to this outstanding importance, a large number of experimental studies and physical models have been devoted to the mechanics of wet granular matter, e.g. [11–16]. The transport of stresses in a dry granulate is governed by an interplay of frictional and repulsive forces acting between the constituting grains. Dry granulates easily flow under external forces such as gravity and hardly resist to shear. However, a confining stress applied to the grains at the surface of the assembly can reversibly turn a dry granulate into a solid-like material [17]. But not only externally applied confining stresses can alter the mechanics of granular assemblies. After mixing dry grains with a small amount of a wetting liquid, the granular assembly turns into a plastically deformable material, which can sustain finite tensile and shear stresses [18].

In this Letter, we explore the rheological behavior of dry and wet granulates by determining the energy that is dissipated while shearing the granulates. To this end, we compare experimental results with results from Discrete Element Simulations (DES), as a function of an external pressure confining the granulate. We unravel the contribution of energy dissipation mechanisms by direct particle-particle interaction (friction, inelastic interactions) and by breaking and reformation of capillary bridges. The main finding is that, for small applied pressures, the energy dissipated during the process of breakage and reformation capillary bridges is the main source of energy dissipation in a wet granulate, dominating both the dissipation due to direct particle–particle interaction and the dissipation arising in the presence of internal cohesion. However, for large applied pressure, friction dominates the particle–particle interaction for both wet

and dry granulates. Accordingly, the work to shear a dry granulate becomes larger than that to shear a wet one for sufficiently large confining pressure.

Experimental Techniques. Throughout this work we employ spherical glass beads with diameters $125 \mu\text{m} \leq d \leq 150 \mu\text{m}$, average diameter $\bar{d} \approx 140 \mu\text{m}$, and polydispersity of $\Delta d/\bar{d} = 0.10$ (Whitehouse Scientific Ltd., UK) as a model granulate. Dense granular assemblies are prepared with a water content of $W = (2.5 \pm 0.5) \text{ vol.}\%$ with respect to the total volume of the granular sample. The advancing contact angle of water on the glass beads is $\theta = (7 \pm 3)^\circ$, as measured by optical goniometry (OCA 20, Data Physics, Germany). Considering the large surface to volume ratio of the capillary bridges in a bead pack, we assume a realistic interfacial tension of $\sigma = 55 \text{ mN/m}$ to account for traces of surface active substances in the water. The friction coefficient of glass beads on a glass microscopy slide was determined to $\mu_{dry} = 0.29 \pm 0.05$ for a dry contact and to $\mu_{wet} = 0.25 \pm 0.04$ for a contact in water, respectively, see Supplemental Materials (SM).

The resistance of wet and dry granular bead assemblies against externally imposed mechanical deformations is determined using a custom made shear cell similar to that one described in [10, 12], cf. Fig. 1a. The central part of the shear cell consists of a cylinder with an inner diameter of $D = 30 \text{ mm}$ and height $H = 10 \text{ mm}$. This cylinder is delimited to both sides by rubber membranes separating the cell volume from two pressure chambers containing water. The granulates are sheared at isochoric conditions. For simplicity, we chose a triangular signal with period T for the dispensed volume $\Delta V(t)$, leading to a constant volume flux between the turning points at $\pm \Delta V_{\text{max}}$. The shear rate in our experiments was sufficiently small to ensure that the Laplace pressure of the capillary bridges can be considered as equilibrated [1], see SM for further details.

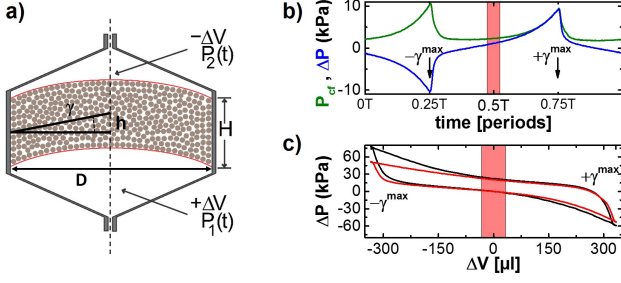


FIG. 1. a) Schematic of the shear cell. b) Differential pressure ΔP and confining pressure P_{cf} recorded during one shear cycle with period T . c) ΔP for one shear cycle re-plotted as a function of volume displacement ΔV , revealing a characteristic hysteresis loop. Data are shown for dry (black) and wet (red, $W = (2.5 \pm 0.5) \text{ vol.}\%$) glass beads for an initial confining pressure of $P_{cf} \approx 33 \text{ kPa}$ at $\Delta V = 0$. The intervals of $P_{cf} \approx \text{const.}$ which are used to analyze the data are indicated by vertical boxes in b) and c).

The differential pressure signal $\Delta P = P_2 - P_1$ recorded during one shear cycle is shown in Fig. 1b. The pressure difference ΔP as a function of volume displacement, ΔV , shown in Fig. 1c, reveals a closed loop for both dry and wet granulate in a stationary shear cycle. The finite area enclosed represents the energy that is dissipated in the system over a shear cycle $E_{\text{diss}} = \oint \Delta P(\Delta V) d\Delta V$ and, thus, reflects the resistance of the granular assembly to the imposed shear deformation. The confining pressure $P_{cf} = (P_1 + P_2)/2$ is about constant around the neutral position of the membranes where $\Delta V = 0$ but increases when approaching the turning points of the shear motion. Thus we restrict the following analysis to the central area of the hysteresis loop with $|\Delta V| \leq 33 \mu\text{l}$ corresponding to a reference shear angle of $\gamma = 2h/D = \pm 0.36^\circ$, where the variation of P_{cf} is small compared to the average of P_{cf} over the considered volume interval. A constant confining pressure is also realized by the design of the DES discussed below.

During shear the glass beads rearrange, resulting in a continuous stretching and eventually in the break-up and reformation of capillary bridges. To determine the number of breaking and re-forming capillary bridges during shear, this process is imaged in 3D by *in situ* X-ray tomography (ID-15A, ESRF) in a downsized shear cell with inner diameter $D = 8.0 \text{ mm}$ and height $H = 4.5 \text{ mm}$, adapted to the geometry of the X-ray beam, cf. Fig. 2 and SM. To reach the resolution required, the tomographic experiments are conducted with larger beads of $250 \mu\text{m} \leq d \leq 300 \mu\text{m}$, $\bar{d} \approx 282 \mu\text{m}$, $\Delta d/\bar{d} = 0.10$.

Simulation techniques. DES were carried out to complement the experiments. For simplicity we perform simulations in a two-dimensional (2D) setup and do not focus on reproducing the experimental conditions precisely; instead we concentrate on qualitative match of the experiments and simulations underlining a generic nature

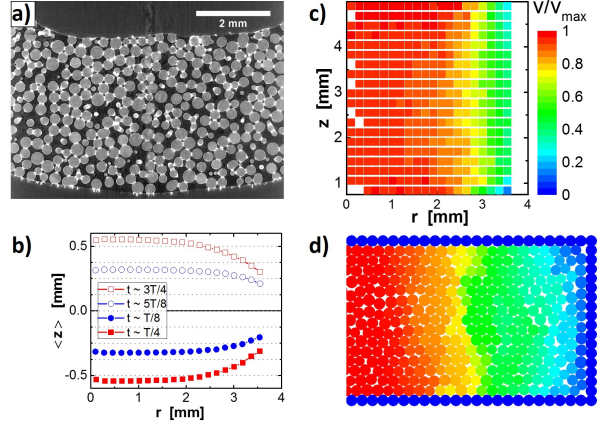


FIG. 2. a) 2D slice through a 3D tomography of a sheared wet bead assembly; liquid capillary bridges appear white. b) Axial bead displacement $\langle z \rangle$ obtained by averaging individual bead displacements in axial and azimuthal direction. c), d) Azimuthal averaged velocity profiles $v(r)$ at zero crossing ($\gamma = 0$) normalized by the maximum shearing velocity v_{max} obtained in experiments c) and DE simulation d).

of the findings. The details of the techniques could be found in e.g. Ref. [21] and SM. We express all the quantities used in simulations in terms of the following scales: \bar{d} as length-scale, average particle mass, m , as mass scale, and the binary particle collision time, $\tau_c = \pi\sqrt{\bar{d}/2gk_n}$, as time scale. The parameter k_n corresponds to the normal spring constant between two colliding particles and g is the acceleration of gravity. The parameters entering the linear force model can be connected to physical properties (Young modulus, Poisson ratio) as described, e.g. in Ref. [22]. The inter-particle friction coefficient for dry and wet disk assemblies is consistent with the experimental values. Furthermore, we use $k_n = 4 \times 10^3$, and the coefficient of restitution, measuring inelasticity of the collisions, is $e = 0.5$. The simulation domain is initially rectangular and of the size 47×17 ; the walls are composed of monodisperse particles of size \bar{d} . The system particles are chosen randomly from a uniform distribution with mean \bar{d} and width $0.4\bar{d}$, cf. Fig. 2d.

In modeling cohesion, we are motivated by the experimental setup for the mechanical measurements. Driven by the minimization of interfacial energies, liquid morphologies form at mutual contacts of neighboring beads or disks. The force of a capillary bridge is taken from Ref. [7]. Capillary bridge area is set to 4 *area%* of average particle disk area corresponding to the 2.5 *vol%* used in the experiments. Bridges are assumed to have equal and constant volume and the contact angle of $\theta = 12^\circ$. A bridge forms after two particles touch and breaks when the bridge length exceeds the maximum one, S^{max} . The energy dissipated during full cycle of formation and rupture is computed by integrating the bridge force F_c up to S^{max} , $E_{\text{cb}}^{\text{single}} = \int_0^{S^{\text{max}}} F_c(S) dS$; cf. SM.

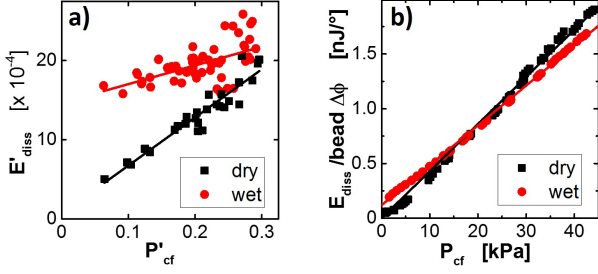


FIG. 3. Dissipated Energy during shear as function of the confining pressure for dry beads (black squares) and wet beads (red circles) a) Numerical results averaged over 15 cycles. For the wet system, $E'_{\text{diss}} = E'_\ell + E'_{\text{cb}}$, see. Eq. (1) and SM. b) Experimental results normalized per bead and shear angle.

Initially, the particles are placed on a rectangular grid with random velocities. Then, the top and bottom walls are moved inward by applying a pressure until equilibrium is reached, similarly to the experiments. At this point, we start shearing the system by prescribing a parabolic wall shape evolving in time. We let the top wall slide up and down to readjust the pressure until the system reaches a stationary shear cycle. Then, we fix the end points of both walls and continue shearing until the pressure inside of the system, averaged over a shear cycle, reaches a constant value. In the discussion that follows, we will use the average value of the pressure on top and bottom wall exerted by the system particles, P'_1 and P'_2 , respectively, to define the confining pressure, P'_{cf} , as in the experiments. To avoid confusion we use a primed notation for simulation (dimensionless) quantities. The (dimensionless) shearing velocity has a cosine profile with the amplitude $v'_s = 10^{-4}$; no significant influence of v_s on the results was observed, cf. SM.

Results. The simulation results provide detailed insight regarding the sources of energy dissipation. To start with, we focus on energies, and correlate the energy input by moving walls $E'_w(t)$ to the various mechanisms for energy dissipation: the difference of elastic (due to compression of particles), kinetic and capillary energies stored in capillary bridges in consecutive time steps, denoted by $\Delta E'_{\text{el}}(t)$, $\Delta E'_k(t)$, $\Delta E'_c(t)$, respectively. The energy dissipated due to friction and inelastic collisions is denoted by $E'_\ell(t)$ and the energy dissipated by breaking of the bridges, $E'_{\text{cb}}(t) = N'_{\text{cb}} \times E'^{\text{single}}_{\text{cb}}$, where N'_{cb} is the total number of broken bridges during a time step. The energy balance is then given by

$$E'_w(t) = \Delta E'_{\text{el}}(t) + \Delta E'_k(t) + \Delta E'_c(t) + E'_\ell(t) + E'_{\text{cb}}(t) \quad (1)$$

We ignore the energy dissipation due to viscous effects, as appropriate for the slow shear rates considered [10].

Equation (1) allows to compute the energy dissipation for both wet and dry disk assemblies (in the dry case, both E'_c , E'_{cb} are trivially zero). Figure 3a shows the

total dissipated energy, $E'_{\text{diss}} = E'_\ell + E'_{\text{cb}}$, averaged over a (stationary) shear cycle, for both wet and dry assemblies. We note that it is difficult to carry out simulations for $P'_{\text{cf}} \lesssim 0.06$ since the particles may detach from the walls. In any case, the trend of the data clearly suggests that for the wet disk assembly, the energy dissipated for $P'_{\text{cf}} \approx 0$, has a non-zero value, while $E'_{\text{diss}} \approx 0$ for the dry case. The amount of the energy dissipated by breaking of the bridges per shear cycle can be computed directly from the number of bridges in the consecutive time steps.

Figure 4a shows the energy dissipated in breaking and reformation of capillary bridges, E'_{cb} , and by friction and inelastic collisions, E'_ℓ . We observe that there is a crossover between the regime where the energy is dissipated mainly in the breaking and reformation bridges for small P'_{cf} , and mostly from friction and inelastic collisions for sufficiently large P'_{cf} . We note that the energy dissipated by breaking and reformation of the bridges is decreasing with the increasing value of P'_{cf} . This finding can be rationalized as follows: at larger confining pressure, particles have less space to move and therefore there are fewer bridges that break. To support this explanation, we compute the non-affine motion, using the approach described in [12]. Figure 4b shows the rescaled non-affine motion as a function of P'_{cf} , averaged over 15 cycles. An overall decreasing trend of the non-affine motion is obvious. We have verified that a modest increase in particle stiffness does not influence the non-affine results. In SM we discuss briefly how friction and particle inelasticity influence non-affine motion.

Another manner in which cohesion can influence energy dissipation is internal cohesion – capillary bridges pull particles together, leading to an enhanced friction at the contacts as well as damping due to inelasticity (see SM) that may influence the energy dissipation through changing E'_ℓ in Eq. (1). To compute this effect, we proceed as follows (cf. also SM): In equilibrium, the capillary force between the particles leads to a compressive force and an overall elastic energy $E'_{\text{el}} \approx 10^{-6}$. Then, we carry out simulations with dry systems and find that this value of elastic energy corresponds to $P'_{\text{cf}} \approx 0.07$. This value of P'_{cf} leads to $E'_\ell \approx 5 \times 10^{-4}$, see Fig. 4a, being less than a third of the energy dissipated by breaking and reformation of capillary bridges, E'_{cb} . Therefore, the results of our simulations suggest that the breakup of capillary bridges, and not the friction or the inelasticity of collisions, is the main source of energy dissipation in weakly compressed systems.

In what follows we compare the findings from simulation with the experimental results. Figure 3b shows the energy dissipated in the experiments, $\Delta E'_{\text{diss}} / \Delta\gamma$, as a function of P_{cf} for dry and wet glass beads. For subsequent comparison with the data obtained by X-ray measurements, $\Delta E'_{\text{diss}}$ is normalized per bead and reference shear angle. As in the simulations, the increase of dissipated energy with increasing P_{cf} is steeper for dry

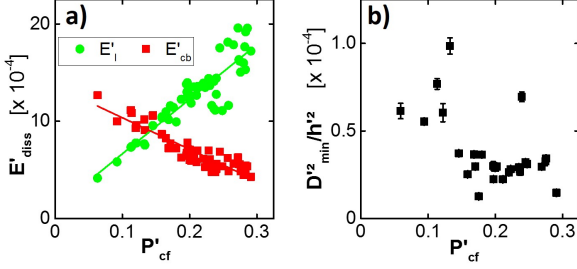


FIG. 4. Numerical results: a) Energy dissipation from breaking and reformation of the bridges and other non-linear effects as a function of P'_{cf} and b) non-affine motion in the system. The results of both panels a) and b) were averaged over 15 cycles for each P'_{cf} .

granulate compared to the wet one. We also find a cross-over, where more energy is dissipated when shearing a wet granulate for small P_{cf} , and where more energy is dissipated shearing a dry granulate for sufficiently large P_{cf} . Both experimentally determined dependencies of the dissipated energy on P_{cf} are consistent with constant slopes $\alpha = dE_{\text{diss}}/dP_{\text{cf}}$ with $\alpha_{\text{dry}} \approx 0.043 \text{ nJ}/(^{\circ}) \text{ kPa}$ and $\alpha_{\text{wet}} \approx 0.036 \text{ nJ}/(^{\circ}) \text{ kPa}$, respectively. Thus, it appears that the slopes of the dissipated energy for increasing P_{cf} correlate to the friction coefficients of the dry and wet beads. In fact, the ratio of the observed slopes for wet and dry glass granulates $\alpha_{\text{wet}}/\alpha_{\text{dry}} = 0.82 \pm 0.05$ is consistent with the ratio of the wet and dry friction coefficients, independently measured for glass beads on a microscope slide of $\mu_{\text{wet}}/\mu_{\text{dry}} = 0.86 \pm 0.05$, cf. SM.

The linear fits to the experimental data have intercepts with the energy axis that are effectively zero for the dry granulate, and $E_{\text{diss}} = (0.12 \pm 0.1) \text{ nJ}/(^{\circ})$ for wet ones, with the error accounting for uncertainties in filling height and packing density. This finite E_{diss} is obviously governed by the presence of capillary bridges and is expected to result from breaking capillary bridges or from internal cohesion due to capillary bridges enhancing the frictional force between the beads.

The internal isostatic cohesion pressure by virtue of capillary forces can be estimated for our system to $\approx 1.2 \text{ kPa}$ using the experimental findings of Scheel [8]. This value is close to the prediction by the Rumpf-Model [26] of $\approx 1.8 \text{ kPa}$. Assuming the cohesion to act similarly to the confining pressure, as also done for simulations, we can use the data of Fig. 3b to estimate the upper bound for the energy dissipated due to friction induced by internal cohesion to $E_{\ell, \text{coh.}} \approx 0.06 \text{ nJ}/(^{\circ})$ per bead.

In the following, we will argue that the remaining energy dissipation for $P_{\text{cf}} \approx 0$ is in fact due to the energy dissipated by forming and breaking of capillary bridges, E_{cb} . The dissipated energy for an individual rupture event, $E_{\text{cb}}^{\text{single}}$ is a function of rescaled liquid bridge volume which is set to $0.00725 d^3$ corresponding

to a liquid content of 2.5 vol.% [8, 14] in our experiments. From the 3D tomography time series (carried out in the small cell), we compute the cumulative number of capillary bridges that rupture between the reference shear angles $\gamma = \pm 0.36^{\circ}$ corresponding to the end of the volume interval in the center of the hysteresis loop shown in Fig. 1c. The number of breaking bridges per bead and reference shear angle is thus determined to be $N_{\text{cb}} \approx 0.208/(^{\circ})$. To allow a comparison to the experimental data obtained using the large cell, we assume that this number is independent of the size of the beads or the dimension of the shear cell. Employing $E_{\text{cb}}^{\text{single}}$, we finally obtain the energy dissipated in breaking and reformation of capillary bridges for wet glass beads to be $E_{\text{cb}} = E_{\text{cb}}^{\text{single}} \times N_{\text{cb}} = (0.10 \pm 0.03) \text{ nJ}/(^{\circ})$. The error is mainly introduced by the 3D image analysis and uncertainties in liquid content. Adding the dissipated energy due to enhanced friction in the presence of cohesive forces, we arrive at $E_{\text{diss}} = E_{\text{cb}} + E_{\ell, \text{coh}} = (0.16 \pm 0.03) \text{ nJ}/(^{\circ})$ for $P_{\text{cf}} \approx 0$. This value agrees nicely with the intercept of the linear fit to the E_{diss}/γ vs. P_{cf} of $(0.12 \pm 0.01) \text{ nJ}/(^{\circ})$ shown in Fig. 3b and with the simulation results that about 2/3 of the energy at $P_{\text{cf}} \approx 0$ is dissipated by breaking capillary bridges.

Conclusion. We explained the origin of energy dissipation in sheared wet and dry granulates consistently by numerical simulations and experimental results. For vanishing externally applied confining pressure, wet granulates are stiffer than dry granulates due to the cohesion by virtue of capillary bridges formed between neighboring beads, which increase the energy dissipation in two ways. About two thirds of the dissipated energy was found to result from breaking capillary bridges which were elongated above their maximum length. The remaining one third is caused by the cohesion which increases the contact forces between beads and thus causes friction even in an unconfined wet granulate. An increase of applied confining pressure is found to have two consequences. First, the simulations show that energy dissipation due to breakup of capillary bridges becomes less relevant due to a decrease of the non-affine particle motion. Second, the energy dissipation for both dry and wet granulates increases due to increased particle-particle friction. Thus for sufficiently large confining pressure energy dissipation is always dominated by friction between grains. Moreover, as the friction coefficient is smaller for wet contacts, a cross-over is observed and more energy is dissipated when dry granulates are sheared at sufficiently large confining pressure.

We acknowledge the support by: the German Research Foundation (DFG) via GRK - 1276, Saarland University (SK, RS) and SPP 1486 “PiKo” under Grant No. HE 2016/14-2 (MB); by a start up grant from Saarland University (ALS); and by the NSF Grant No. DMS-1521717 and DARPA contract No. HR0011-16-2-0033 (LK, LK).

Supplemental Materials: Energy dissipation in sheared wet granular assemblies

Experiments

Determination of Friction Coefficients The sliding friction coefficients of $\mu_{wet} = 0.25 \pm 0.04$ and $\mu_{dry} = 0.29 \pm 0.05$ for dry and wet friction were measured between the same type of glass spheres as used for the granular experiments and a glass microscopy slide. For that three glass beads were fixed at the bottom side of a triangular plastic sheet and loaded with a weight of known mass. The sliding friction was determined from the constant velocity of this tripod when sliding down the tilted microscopy slide. As the surface of the glass slide is smoother than the surface of the beads the values might be considered as lower estimates of the friction coefficients between glass beads.

Further details of the shear cells Two shear cells were used for the experiments: a larger one providing high quality mechanical data and a down sized version that fitted into the available X-ray beam to enable in-situ monitoring of the rearrangement of beads and liquid during shear. Both shear cells were machined from solid blocks of polycarbonate. The latex membranes with a thickness of $300 \mu m$ were fixed to the pressure chambers by ergo 5925 superglue. The pressure chambers and the entire tubing system were carefully filled with degassed water to avoid any trapped air bubbles. One of the pressure chambers was fixed to the central part of the shear cell and the shear cell was filled in horizontal position with dry or wet granulate. Subsequently, the shear cell was closed with the second pressure chamber.

The pressures in each chamber P_1 and P_2 and the differential pressure between these two chambers $\Delta P = P_2 - P_1$ were monitored by calibrated pressure transducers (24 PCD, sensitivity: 11 mV per psi, Honeywell). The pressure chambers were connected by PTFE tubing to precision microliter syringes (Hamilton-1002 TLL) driven by computer-controlled syringe pumps. The desired initial confining pressure $P_{cf} = (P_1 + P_2)/2$ is adjusted by adding or withdrawing an identical volume of liquid to or from both chambers. To ensure that the pressure applied to the granulate and not to the gas phase, the cylindrical core has an opening to allow for air exchange but small enough so that no beads can escape. Before recording shear cycles the granulate was sheared several times to adjust its packing density and to obtain a confining pressure P_{cf} that is stable for several shear cycles. The granulates are sheared at isochoric condition by simultaneously increasing the volume of one chamber by the same volume ΔV that is withdrawn from the other chamber. A cross section through a tomogram of a sheared granulate and the shear displacement of the beads as analyzed from the X-ray tomography time se-

- [1] A. Faure, P. York and R. C. Rowe, *Eur. J. Pharm. Biopharm.* **52**, 269–277 (2001).
- [2] H. Leuenberger, *Eur. J. Pharm. Biopharm.* **52**, 279–288 (2001).
- [3] H. Leuenberger, *Eur. J. Pharm. Biopharm.* **52**, 289–296 (2001).
- [4] W. Paul and C. P. Sharma, *J. Mater. Sci. Mater. Med.* **10**, 383–388 (1999).
- [5] V. S. Komlev, S. M. Barinov and E. V. Koplik, *Biomaterials* **23**, 3449–3454 (2002).
- [6] S. J. R. Simons and R. J. Fairbrother, *Powder Technol.* **110** 44–58 (2000).
- [7] J. Litster and B. Ennis, *The Science and Engineering of Granulation Processes Particle Technologies Series, Springer Netherlands*, 2004.
- [8] A. Realpe and C. Velázquez, *Chem. Eng. Sci.* **63**, 1602–1611 (2008).
- [9] K. Shinagawa and Y. Hirashima, *Met. Mater. Int.* **4**, 350–353 (1998).
- [10] B. Bhandari, N. Bansal, M. Zhang and P. Schuck, *Handbook of Food Powders*, ISBN: 978-0-85709-513-8, Woodhead Publishing (2013).
- [11] J. C. Géminard, W. Losert and J. P. Gollub, *Phys. Rev. E* **59**, 5881–5890 (1999).
- [12] Z. Fournier *et al.*, *J. Phys.: Condens. Matter* **17**, S477 (2005).
- [13] N. Mitarai and F. Nori, *Adv. Phys.* **55**, 1–2 (2006).
- [14] M. Scheel, R. Seemann, M. Brinkmann, M. Di Michiel, A. Sheppard, B. Breidenbach and S. Herminghaus, *Nat. Mater.* **7**, 189 (2008).
- [15] J. E. Fiscina, M. Pakpour, A. Fall, N. Vandewalle, C. Wagner and D. Bonn, *Phys. Rev. E* **86**, 020103 (R) (2012).
- [16] A. Fall, B. Weber, M. Pakpour, N. Lenoir, N. Shahidzadeh, J. Fiscina, C. Wagner and D. Bonn, *Phys. Rev. Lett.* **112**, 175502 (2014).
- [17] E. Brown, N. Rodenberg, J. Amend, A. Mozeika, E. Steltz, M. R. Zakin, H. Lipson, and H. M. Jaeger, *Proc. Natl. Acad. Sci. USA*, **107**, 18809 (2010).
- [18] T. C. Halsey and A. J. Levine, *Phys. Rev. Lett.* **80**, 3141 (1998).
- [19] S. Herminghaus, *Adv. Phys.* **54**, 221 (2005).
- [20] R. Mani, C. Semperebon, D. Kadau, H. J. Herrmann, M. Brinkmann and S. Herminghaus, *Phys. Rev. E* **91**, 042204, (2015).
- [21] L. Kovalcinova, A. Goulet and L. Kondic, *Phys. Rev. E* **92**, 032204, (2015).
- [22] L. Kondic, *Phys. Rev. E* **60**, 751–770 (1999).
- [23] C. D. Willett, M. J. Adams, S. A. Johnson and J. P. K. Seville, *Langmuir* **16** 9396–9405 (2000).
- [24] L. Kondic, X. Fang, W. Losert, C.S. O’Hern and R.P. Behringer, *Phys. Rev. E* **85**, 011305 (2012).
- [25] M. Scheel, R. Seemann, M. Brinkmann, M. Di Michiel, A. Sheppard and S. Herminghaus, *J. Phys.: Condens. Matter* **20**, 49 (2008).
- [26] H. Rumpf *et al.*, *Agglomerations*, Edited by W. A. Knepper (Interscience, New York), p. 379–413 (1962).
- [SM] See Supplemental Material at [URL will be inserted by publisher] for additional experimental and computational details.

ries are shown in Fig. 2a,b of the main text. The resulting small displacement $h \ll D$ in the center of the cylindrical cell was used to approximate the reference shear angle γ and the 2D shear rate $\dot{\gamma}$ by $\gamma = 2h/D$ and $\dot{\gamma} = 2h/(DT)$. The average applied reference shear rate in our experiments was fixed to $\dot{\gamma} \approx 3 \times 10^{-3} \text{ s}^{-1}$ and the shear angle reaches $\pm\gamma^{\text{max}} = \pm 3^\circ$ at the turning points for the mechanical tests. The shear rate applied to the small shear cell is $\dot{\gamma} \approx 2 \times 10^{-4} \text{ s}^{-1}$, i.e. about one order of magnitude lower than for the large shear cell. When considering the dependence of the liquid exchange time on the diameter ($t \propto d^4$) [S1] the liquid exchange rate in the small shear cell corresponds to a shear rate of $\dot{\gamma} \approx 3 \times 10^{-3} \text{ s}^{-1}$, i.e. comparable to the large shear cell and in particular also in the quasi static limit. Instead of pure water, used as wetting liquid in the large shear cell, KI (1.56 g/cm^3) was added to the water which is used in the small shear cell. KI increases the X-ray absorption without noticeable effects on contact angle and surface tension compared to pure water.

Further details of computed X-ray tomography

The in situ X-ray imaging was done using a monochromatic parallel X-ray beam [S2] from an undulator source with X-ray energies of about 50 keV with a pixel resolution of $5.5 \text{ } \mu\text{m}/\text{pixel}$. A full 3D tomogram is recorded within 4 seconds capturing 4000 absorption projections while the sample is rotated by 180° . During a full shear cycle, 32 tomograms were recorded with a time interval of 104.3 sec.

The 3D gray scale tomographic images are reconstructed using a standard filtered back-projection algorithm. Image post-processing steps, like edge-preserving anisotropic diffusion filtering [S3] and segmenting the different phases [S4, S5] into distinct binary images, are conducted with the 3D volume toolkit Mango [S6]. Further analysis of the segmented tomograms is conducted with various built-in algorithms of the Mango toolkit and custom MatlabTM scripts.

Scaling the results from the small shear cell with larger beads to the bigger cell with smaller beads For a quantitative comparison of the results obtained for a certain shear angle $\Delta\gamma$ for the small shear cell (with beads of $d = 282 \text{ } \mu\text{m}$) with the mechanical data of the large shear cell (using beads with $d = 140 \text{ } \mu\text{m}$), we have to scale ΔE_{diss} per bead with the respective bead diameter. For a constant shear angle, the number of breaking bridges per bead is assumed to be independent on the bead size and the dissipated energy to scale linearly with the number of beads in the granular volume assuming a constant packing density of ≈ 0.58 and the dissipated energy for a breaking bridge $E_{\text{cb}}^{\text{single}} = \int_0^{S^{\text{max}}} F_c(S) \text{ d}S$. The energy dissipated upon bridge rupture $E_{\text{cb}}^{\text{single}}$ for a certain bead diameter and liquid content can be calculated by integrating the bridge force $F_c(S)$ from eq. A1

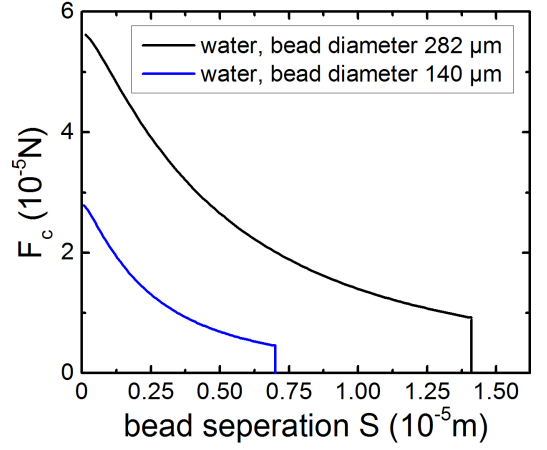


FIG. S1. Capillary bridge force F_c as function of surface separation distance S for a fixed liquid volume $V/d^3 = 0.00725$ replotted from eq. A1 in Ref. [S7]. The liquid volume is set to $V = 0.00725 d^3$ corresponding to the largest possible capillary bridge [S8].

in Ref. [S7] (c.f. Fig. S1) from zero separation $S = 0$ to the rupture distance S^{max} see also further details given below.

Simulations

Force Model The particles in the considered numerical system are modeled as 2D soft frictional inelastic disks that interact via normal and tangential forces, specified here in nondimensional form, using \bar{d} , m , τ_c as the length, mass and time scale introduced in the main body of the paper. We denote the (simulation) dimensionless quantities using prime to distinguish from corresponding experimental measures.

Dimensionless normal force between i -th and j -th particle is

$$\mathbf{F}_{i,j}^{n'} = k'_n x'_{i,j} \mathbf{n} - \eta'_n \bar{m}' \mathbf{v}_{i,j}^{n'}, \quad (\text{S1})$$

where $\mathbf{v}_{i,j}^{n'}$ is the relative normal velocity, \bar{m}' is reduced mass, $x'_{i,j} = d'_{\text{ave}} - r'_{i,j}$ is the amount of compression, with $d'_{\text{ave}} = (d'_i + d'_j)/2$ and d'_i , d'_j diameters of the particles i and j . The distance of the centers of i -th and j -th particle is denoted as $r'_{i,j}$. Parameter η'_n is the damping coefficient in the normal direction, related to the coefficient of restitution e .

We implement the Cundall–Strack model for static friction [S9]. The tangential spring ξ' is introduced between particles for each new contact that forms at time $T = T_0$ and is used to determine the tangential force during the contact of particles. Due to the relative motion of particles, the spring length ξ' evolves as $\xi' = \int_{T_0}^T \mathbf{v}_{i,j}^{t'}(t') dt'$ with $\mathbf{v}_{i,j}^{t'} = \mathbf{v}'_{i,j} - \mathbf{v}'_{j,i}$ and $\mathbf{v}'_{i,j}$ being the relative velocity of particles i , j . The tangential direction is defined as $\mathbf{t} = \mathbf{v}_{i,j}^{t'}/|\mathbf{v}_{i,j}^{t'}|$. The direction of

ξ' evolves over time and we thus correct the tangential spring as $\xi'' = \xi' - \mathbf{n}(\mathbf{n} \cdot \xi')$. The tangential force is set to

$$\mathbf{F}^{t'} = \min(\mu_s |\mathbf{F}^{n'}|, |\mathbf{F}^{t'*}|) \mathbf{F}^{t'*} / |\mathbf{F}^{t'*}|, \quad (\text{S2})$$

with

$$\mathbf{F}^{t'*} = -k'_t \xi'' - \eta'_t \bar{m}' \mathbf{v}_{i,j}^{t'}. \quad (\text{S3})$$

Viscous damping in the tangential direction is included in the model via the damping coefficient $\eta'_t = \eta'_n$.

The value of the normal spring constant (in terms of mg/\bar{d}) is $k'_n = 4 \times 10^3$. Parameters η'_n and k'_t are set to $\eta'_n = 1.4$ (consistent with $e = 0.5$ specified in the main body of the paper) and $k'_t = 0.8k'_n$. The inter-particle friction coefficient μ_s for the dry and wet assemblies is set to the (experimental) values $\mu_{\text{dry}} = 0.29$ and $\mu_{\text{wet}} = 0.25$, respectively, and the shearing velocity has a cosine profile with the amplitude $v'_s = \dot{\gamma}' L' = 10^{-4}$, where $\dot{\gamma}'$ is the shear rate and $L' = 47$ is the length of the shear cell.

Capillary Interactions Additional attractive (capillary) forces arise from the capillary bridges that form when particles come into contact. The capillary forces are modeled using the approach outlined in Ref. [S7, S10]. We motivate the choice of the force model between 3D spheres by the effort to use the same type of cohesive interaction between particles as in the experiments. Note that according to [S11], cohesive force in 2D assumes a local maximum at a non-zero distance of the particles, in contrast to the 3D model. Furthermore, to simplify the implementation, we use the approximate expression, Eq. (12) in [S10]

$$F'_{c,ij} = \frac{\pi d' \sigma' \cos \theta}{1 + 1.05 \hat{S}_{ij} + 2.5 \hat{S}_{ij}^2}, \quad (\text{S4})$$

where $\hat{S}_{ij} = S'_{ij} \sqrt{d'/2V'}$ and $S'_{ij} = r'_{ij} - (d'_i + d'_j)/2$ (taken to be 0 whenever particles are in contact) is the particle separation where r'_{ij} is the distance between the centers of the particles i, j . The inverse value of the reduced diameter is $1/d' = (1/d'_i + 1/d'_j)/2$ and d'_i, d'_j are the diameters of the particles. For the contact angle, θ , and the surface tension, $\sigma = \sigma' m/\tau_c^2$, we use the standard values for water (12° , 72 mN/m); the influence of the slightly different choice of parameters compared to the ones appropriate to the experiments is minor for the present purposes. The maximum separating distance $S^{\text{max}'}$ at which a bridge breaks is given by

$$S^{\text{max}'} = (2 + \theta) \left(\frac{V'^{1/3}}{d'} + \frac{2V'^{2/3}}{d'^2} \right), \quad (\text{S5})$$

where V' is the non-dimensional capillary bridge volume. The approximation of a volume of capillary bridge is obtained by rotating the liquid bridge area between disks around its axis of symmetry. The total liquid area in

the granular assembly is $\approx 4\%$ of the total particle area, corresponding to appropriately 2.5% of total system area.

Energies in Sheared Granular Assembly

Energy Entering the Shear Cell Through Moving Walls During shear, the top and bottom walls have a prescribed parabolic shape that changes over time, and left and right boundaries are fixed. To compute the energy that is added to the system by moving the walls, one has to integrate the force over the boundary. There is no energy added to the system through the (fixed) left and right wall and we only need to find the energy entering through the collision of assembly particles with the top and bottom wall. This energy is given by

$$E'_w = \sum_j \mathbf{F}'_j \cdot \mathbf{n}_j ds, \quad (\text{S6})$$

where j sums over all collisions of the bottom and top wall particles with any of the assembly particles. Here, \mathbf{n}_j is the unit vector normal to the boundary at the location of the wall particle experiencing a collision, \mathbf{F}'_j is the force on the wall particle and ds is the length element (here the wall particle diameter).

The motion of the top and bottom wall is periodic in time with period T' (time is expressed in dimensionless units). During the time $t \in (-T'/4, 3T'/4]$, the vertical position of top and bottom boundary is given by

$$y(t') = \left(1 - \frac{2x^2}{L'} \right) t' v' + C \quad \text{for } t' \in (-T'/4, T'/4] \quad (\text{S7})$$

$$y(t') = \left(1 - \frac{2x^2}{L'} \right) (T' - t') v' + C \quad \text{for } t' \in (T'/4, 3T'/4] \quad (\text{S8})$$

where x is the wall particle coordinate with respect to the horizontal axis (assuming that $x = 0$ for the center of the top/bottom wall), y is the vertical axis coordinate of the wall particle at time t' and the shearing velocity v' has a cosine profile. The amplitude of $|v'|$ over the shear cycle is shearing velocity, v'_s , introduced in the main body of the paper; the constant C assumes the appropriate value for the top and bottom wall particles.

For the direction normal to the boundary at the center of the particle w_j , we have $\mathbf{n}_j \cdot \mathbf{t}_j = 0$ with \mathbf{t}_j being a unit vector tangential to the boundary at w_j . The slope of the curve with the tangent vector \mathbf{t}_j is given by $y'|_{x=x_j} = 2ax_j$, where the value of a is obtained from $y(t)$ and x_j in Eqs. (S7) and (S8). Thus $\mathbf{t}_j = (1\mathbf{e}_x + 2ax_j\mathbf{e}_y)/(1 + 4a^2x_j^2)^{1/2}$ and the unit normal vector \mathbf{n}_j is given by

$$\mathbf{n}_j = \frac{(-2ax_j\mathbf{e}_x + \mathbf{e}_y)}{\sqrt{1 + 4a^2x_j^2}} \quad (\text{S9})$$

Finally, we obtain the expression for the total energy added to the system by the moving walls

$$\begin{aligned} E'_w &= \sum_j \mathbf{F}'_j \cdot \mathbf{n}_j ds \\ &= \sum_j \frac{(-2ax_j \mathbf{e}_x + 1\mathbf{e}_y)}{\sqrt{1+4a^2x_j^2}} \cdot \mathbf{F}'_j ds. \end{aligned} \quad (\text{S10})$$

Total capillary energy stored in capillary bridge(s) between the particles i, j , can be found by integrating the force between them over the separating distance S' (smaller than the maximum separating distance $S^{\max'}$)

$$E'_c{}^{i,j} = \int_0^{S'} |\mathbf{F}'_{c,ij}| dS \quad (\text{S11})$$

$$(\text{S12})$$

with the functional form of $|\mathbf{F}'_{c,ij}|$ given in Eq. (S4). The closed form of the energy stored in a capillary bridge is

$$\begin{aligned} E'_c{}^{i,j} &= 4\pi\sigma' \cos(\theta) \sqrt{\frac{d'V'}{2\epsilon}} \left[\arctan \left\{ 5\bar{S}' \sqrt{\frac{d'}{2V'\epsilon}} + \frac{\delta}{\sqrt{\epsilon}} \right\} \right. \\ &\quad \left. - \arctan \left\{ \frac{\delta}{\sqrt{\epsilon}} \right\} \right] \end{aligned}$$

with $\delta = 1.05$ and $\epsilon = 8.8795$. The total energy stored in all capillary bridges is

$$E'_c = \sum_{i,j} E'_c{}^{i,j}, \quad (\text{S13})$$

for all pairs of particles i, j that interact via capillary force.

Energy dissipated due to rupturing of capillary bridges is equal to the capillary energy at the maximum separating distance $S^{\max'}$. To find the total energy dissipated due to breaking and reformation of the bridges, we sum over all ruptured bridges

$$E'_{cb} = \sum_{i,j} \int_0^{S^{\max'}} |\mathbf{F}'_{c,ij}| dS. \quad (\text{S14})$$

The indices i, j refer to all pairs of particles that experienced bridge rupturing.

Kinetic energy is computed as

$$E'_k = \sum_{i=1}^N \frac{m'_i |\mathbf{v}'_i|^2}{2}, \quad (\text{S15})$$

where N is the total number of system particles and m'_i , $|\mathbf{v}'_i|$ are the mass and velocity of the i -th particle, respectively.

Elastic energy is computed as

$$E'_{el} = \sum_{i,j} \frac{k'_n x_{i,j}^2}{2}, \quad (\text{S16})$$

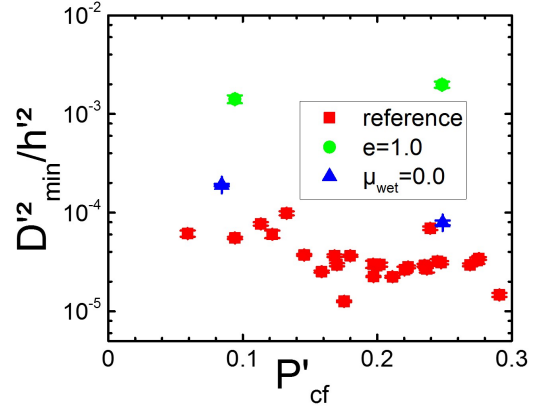


FIG. S2. Non-affine motion rescaled with the squared shear amplitude, $D_{\min}'^2/h'^2$, for the reference (red squares: $\mu_{\text{wet}} = 0.25, e = 0.5$), elastic (green circles: $\mu_{\text{wet}} = 0.25, e = 1$) and frictionless (blue triangles: $\mu_{\text{wet}} = 0, e = 0.5$) assembly of wet particles as a function of confining pressure, P'_{cf} , averaged over 12 cycles.

where i, j runs over all pairs of overlapping particles, including the system particle – wall particle interactions.

Total energy dissipated during a time step can be computed from the following energy balance equation. The energy entering the system due to the moving walls has to be equal to the sum of the changes in the elastic, kinetic and capillary energies, $\Delta E'_{el}(t), \Delta E'_k(t)$ and $\Delta E'_c(t)$, between two consecutive time steps, $(t - \Delta t)$ and t , the energy dissipated by breaking and reformation of capillary bridges $E'_{cb}(t)$ and the energy dissipated due to friction and other non-linear effects, $E'_\ell(t)$. Thus, we have

$$E'_w(t) = \Delta E'_{el}(t) + \Delta E'_{kl}(t) + \Delta E'_c(t) + E'_\ell(t) + E'_{cb}(t). \quad (\text{S17})$$

From Eq. (S17), we can compute the dissipated energy, $E'_{\text{diss}}(t)$. When there is no cohesion in the system, $E'_c, E'_{cb} = 0$ trivially, and we can use the same formula to find E'_{diss} for dry systems.

Non-affine Motion

During shear, the particles move not only in the manner imposed by the moving walls, but also relative to each other. The relative motion of the particles, also referred to as the non-affine motion, is expected to be the main reason for the breaking and reformation of the capillary bridges and subsequently the energy dissipation tied to the capillary effects, E'_{cb} . Therefore, with the particular goal of explaining the decrease of E'_{cb} with increasing P'_{cf} , see Fig. 4a in the main body of the paper, we investigate the non-affine motion of the particles as a function of P'_{cf} (confining pressure), friction and inelasticity. In the

following text we refer to the granular assembly used for simulations in the main body of this paper as the reference system. To compute the non-affine motion, we follow the approach described in Ref. [S12]. First, for every particle p , we find the affine deformation matrix $A'_p(t)$ at the time t with the property

$$A'_p(t)\mathbf{r}'_p(t) = \mathbf{r}'_p(t + \delta t), \quad (\text{S18})$$

where $\mathbf{r}'_p(t)$ is the position of the particle p' at time t . The non-affine motion is defined as the minimum of the mean squared displacement

$$D_{\min}^{\prime 2} = \min \left\{ \sum_{n=1}^m \|\mathbf{r}'_n - \mathbf{r}'_p - [A'_n \mathbf{r}'_n - A'_p \mathbf{r}'_p]\|^2 \right\} \quad (\text{S19})$$

where m is the number of particles within the distance of $2.5d'_{\text{ave}}$ from the particle p , and $\mathbf{r}'_n(t)$ is the position of the n -th particle within this distance.

Figure S2 shows the non-affine motion $D_{\min}^{\prime 2}/h'^2$ for the reference, frictionless and elastic assembly of particles rescaled by the square magnitude of the maximum shearing displacement of the top boundary from the flat position h'^2 as a function of P'_{cf} . We note that for larger pressures, the particles move less relative to each other. Therefore, we expect that the energy dissipation due to breaking of capillary bridges decreases as the pressure increases. Frictionless and elastic assemblies show a significantly larger magnitude of the non-affine motion.

To complete the analysis of the non-affine motion, we clarify the influence of friction and inelasticity of the particles on E'_ℓ and E'_{cb} . We compare the results obtained with the parameters as considered so far (the reference case) to the system with frictionless and elastic particles. Figure S3 shows E'_{cb} , E'_ℓ and the rescaled non-affine motion, $D_{\min}^{\prime 2}/h'^2$, during multiple shear cycles, C_n (non-affine motion averaged over multiple shear cycles shown

also in Fig. S2). The comparison is made for systems with $P'_{\text{cf}} \approx 0.25$, which corresponds to the regime such that the frictional forces dominate the particle-particle interaction (see Fig. 4a in the main body of the paper). We observe once again that the smaller non-affine motion for any of the systems considered corresponds to the smaller E'_{cb} and E'_ℓ while the larger value of non-affine motion corresponds to larger values of E'_{cb} and E'_ℓ .

-
- [S1] R. Mani, C. Semperebon, D. Kadau, H. J. Herrmann, M. Brinkmann and S. Herminghaus, *Phys. Rev. E* **91**, 042204, (2015).
 - [S2] M. Di Michiel, J. M. Merino, D. Fernandez-Carreiras, T. Buslaps, V. Honkimaeki, P. Falus, T. Martins and O. Svensson, *Rev. Sci. Instr.* **76**, 043702 (2005).
 - [S3] A. S. Frangakis and R. Hegerl, *J. Struct. Biol.* **135**, 239-250 (2001).
 - [S4] A. P. Sheppard, R. M. Sok and H. Averdunk, *Physica A* **339**, 145-151 (2004).
 - [S5] J. A. Sethian, Computer Vision and Materials Science, Cambridge University Press (1999).
 - [S6] H. Averdunk and A. Sheppard, *3D image analysis toolkit: Mango* (2010).
 - [S7] C. D. Willett, M. J. Adams, S. A. Johnson and J. P. K. Seville, *Langmuir* **16** 24 9396-9405 (2000).
 - [S8] M. Scheel, R. Seemann, M. Brinkmann, M. Di Michiel, A. Sheppard and S. Herminghaus, *J. Phys.: Condens. Matter* **20**, 49 (2008).
 - [S9] P. A. Cundall and O. D. L. Strack, *Géotechnique* **29** 47-65 (1979).
 - [S10] S. Herminghaus, Dynamics of wet granular matter, *Advances in Physics* **54**, 221 (2005).
 - [S11] M. E. D. Urso and C. J. Lawrence and M. J. Adams, *Journal of Colloid and Interface Science* **220**, 42-56 (1999),
 - [S12] L. Kondic, X. Fang, W. Losert, C.S. O'Hern and R.P. Behringer, *Phys. Rev. E* **85** 011305 (2012).

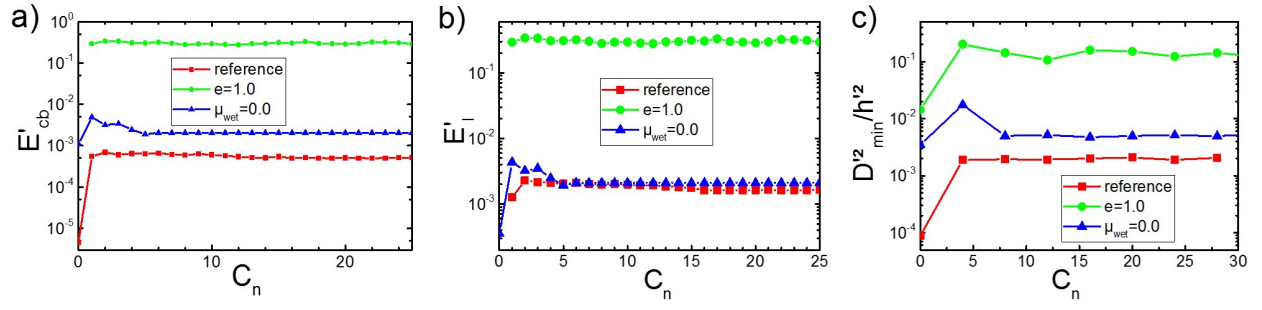


FIG. S3. a) Energy dissipated due to breaking and reformation of the bridges and b) energy dissipated by inelasticity and friction and c) non-affine motion during multiple shearing cycles, C_n , for the reference (red squares: $\mu_{wet} = 0.25, e = 0.5$) case, elastic (green circles: $\mu_{wet} = 0.25, e = 1$) and frictionless (blue triangles: $\mu_{wet} = 0, e = 0.5$) particles with $P'_{cf} \approx 0.25$.